**Astronomy**
**&**
**Astrophysics**

# Acoustic and magnetic wave heating in stars

## I. Theoretical chromospheric models and emerging radiative fluxes

D. Fawzy[1], W. Rammacher[1], P. Ulmschneider[1], Z. E. Musielak[2,1], and K. Stępień[3]

[1] Institut für Theoretische Astrophysik der Universität Heidelberg, Tiergartenstr. 15, 69121 Heidelberg, Germany
[2] Department of Physics, University of Texas at Arlington, Arlington, TX 76019, USA
[3] Warsaw University Observatory, Al. Ujazdowskie 4, 00478 Warszawa, Poland

**Abstract.** We describe a method to construct theoretical, time-dependent, two-component and wave heated chromosphere models for late-type dwarfs. The models depend only on four basic stellar parameters: effective temperature, gravity, metallicity and filling factor, which determines the coverage of these stars by surface magnetic fields. They consist of non-magnetic regions heated by acoustic waves and vertically oriented magnetic flux tubes heated by longitudinal tube waves with contributions from transverse tube waves. Acoustic, longitudinal and transverse wave energy spectra and fluxes generated in stellar convection zones are computed and used as input parameters for the theoretical models. The waves are allowed to propagate and heat both components by shock dissipation. We compute the time-dependent energy balance between the dissipated wave energy and the most prominent chromospheric radiative losses as function of height in the stellar atmosphere. For the flux tube covered stars, the emerging radiative fluxes in the Ca II and Mg II lines are computed by using a newly developed multi-ray radiative transfer method.

**Key words.** methods: numerical – stars: chromospheres – stars: coronae – stars: magnetic fields – MHD – waves

## 1. Introduction

The observations of the Ca II H and K as well as Mg II h and k lines show the presence of core emission in all observed late-type stars. This emission is attributed to an outward temperature rise in the chromospheres of these stars which is ultimately generated by mechanical heating. The observed chromospheric emission depends on the effective temperature and gravity of a star (Wilson 1968; Linsky 1980; Noyes et al. 1984; Schrijver 1987; Stępień 1994; Strassmeier et al. 1994). The fact that stars of the same effective temperature and gravity have different levels of chomospheric emission is attributed to a different coverage of the stars by magnetic fields which in turn is intimately connected with a different stellar rotation period.

Since the stars are uniquely described by four basic parameters, which usually are identified as the effective temperature $T_{\rm eff}$, gravity $g$, metallicity $Z_{\rm M}$, and rotation period $P_{\rm rot}$, the theoretical challenge is to understand the outer structure of stellar atmospheres and the resulting chromospheric radiative emissions as functions of these four fundamental parameters. In principle, there must be such physical connections, however, their full theoretical explanation cannot currently be achieved because of lack

of a first-principle theory of stellar dynamos (e.g., Weiss 1994). As a result, the distribution of magnetic fields on a stellar surface based on the observed stellar rotation rate cannot be theoretically predicted.

Another important but still unsolved problem is to identify the physical processes which are responsible for the heating of stellar atmospheres and explain the chromospheric structure and emission in terms of the stellar surface parameters and the magnetic field coverage. The main aim of this paper is to describe theoretical methods that can be used to address the latter problem and make direct comparisons with observations.

Our approach is to replace the stellar rotation period $P_{\rm rot}$ by a parameter called "filling factor", $f$, which determines the coverage of stars by surface magnetic fields and use this parameter together with $T_{\rm eff}$, $g$ and $Z_{\rm M}$ to construct theoretical chromospheric models which will allow us to simulate the observed chromospheric structure and emission fluxes of late-type stars. It is clear that in order to construct such models, the appropriate heating mechanisms operating in stellar chromospheres must be specified.

According to Narain & Ulmschneider (1996), the various proposed heating mechanisms can be divided into two main categories: hydrodynamic (acoustic and pulsational waves) and magnetic mechanisms (MHD waves and magnetic field dissipation). Currently, the mechanisms which

heat the different layers of stellar atmospheres are still poorly known. However, it has been found by Buchholz et al. (1998) that acoustic wave heating appears to be the basic mechanism for non-magnetic chromospheres. This makes it very likely that a similar mechanism, namely, longitudinal magnetic tube wave heating might work for magnetic regions of stellar chromospheres. It is the purpose of the present series of papers to show that this identification appears to be true. We thus assume that *the acoustic and magnetic wave heating mechanisms dominate in stellar chromospheres and that the wave energy needed for this heating is generated in the stellar convection zones.*

In the present work we outline our methods to simulate chromospheric emission fluxes in the Ca II H+K and Mg II h+k lines by constructing new theoretical, time-dependent and two-component chromosphere models of late-type dwarfs. In a subsequent paper we will use these methods to compare our theoretical emission fluxes with observations and probe the dependence of the emission fluxes on effective temperature as well as the range of stellar activity associated with different magnetic field coverage. This will allow us to determine the role played by acoustic and magnetic wave energy in heating of different regions of stellar atmospheres.

Our paper is organized as follows: Sect. 2 describes the magnetic flux tube forest models used in our computations and the generated wave energy spectra and fluxes in the magnetic and non-magnetic regions of these models. How to construct the initial atmosphere and subsequent chromosphere models is outlined in Sect. 3. In Sect. 4, the method to compute the radiation flux emerging from our two-component models is discussed. Section 5 shows simulated theoretical line profiles and provides emission fluxes, while Sect. 6 gives or conclusions.

## 2. Magnetic flux tube forest model and wave energy generation

### 2.1. Overview of our methods

Since our aim is to compare the observed chromospheric emission fluxes as well as the range of the chromospheric activity with *purely theoretical simulations* based on acoustic and magnetic wave heating, we now describe in detail the theoretical methods employed by us. At first it has to be stressed that *we attempt to obtain theoretical chromospheric emission fluxes with fully ab initio calculations, which are performed by using only the four basic parameters that uniquely characterize main-sequence stars:* effective temperature $T_{\rm eff}$, gravity $g$, metallicity $Z_{\rm M}$, for which we take solar population I values throughout this work, and rotation period $P_{\rm rot}$.

A stellar dynamo theory, which would allow us to predict the magnetic field coverage of the stellar surface for a given choice of the four basic stellar parameters, is not yet available, therefore, we replace the specification of $P_{\rm rot}$ by the assumption of a magnetic area filling factor $f$ that is defined as the ratio of the stellar area covered by magnetic fields to the total area. As the magnetic field spreads with height in the star, the filling factor depends on height. We therefore take the filling factor $f$ at the stellar surface as our fourth basic stellar parameter. Note that the stellar surface is defined by the level where the optical depth at 5000 Å is unity in non-magnetic regions.

Our theoretical approach proceeds as follows. Based on the above four stellar parameters, we compute convection zone models and use them to calculate the generated acoustic and magnetic (longitudinal and transverse) wave energy spectra and fluxes. Assuming a uniform distribution of thin magnetic flux tubes over the stellar surface, we construct magnetic flux tube models based on the assumed filling factor. These tubes spread with height until they completely fill out the stellar atmosphere above a certain height and produce a flux tube forest. With the given wave energy fluxes and spectra, the propagation of the acoustic and magnetic waves is then computed in both the non-magnetic and magnetic regions of stellar atmospheres. The wave dissipation resulting from shocks leads to efficient atmospheric heating, which is locally balanced by chromospheric radiative losses (see Sect. 4.1). Based on the time-dependent energy balance, models of stellar chromospheres are calculated and then used to compute the emerging emission fluxes in the Ca II and Mg II lines.

### 2.2. Stellar convection zone models

To model the subsurface regions of late-type stars we use a convection zone code described by Bohn (1984) and later modified by Theurer (1993) and Ulmschneider et al. (1996). It is assumed that occasionally this convection zone is permeated by thin vertically oriented magnetic flux tubes which do not perturb the non-magnetic medium that surrounds them. The code is based on the mixing-length description of convection, takes into account the formation of hydrogen molecules, and treats radiation transport in the gray LTE approximation; for discussion of the validity of this approximation see Musielak et al. (1994) and Ulmschneider et al. (1999). To run the code, we must specify $T_{\rm eff}$, $g$, the metallicity $Z_{\rm M}$ (solar) and the mixing-length parameter $\alpha = l_{\rm mix}/H$, where $l_{\rm mix}$ is the mixing-length and $H$ the local scale height. A value of $\alpha = 2$ seems to be indicated by time-dependent hydrodynamic simulations of stellar convection (see, for example, Steffen 1993; Trampedach et al. 1997) as well as by a careful fitting of evolutionary tracks of the Sun with its present luminosity, effective temperature and age (Hünsch & Schröder 1997; Schröder & Eggleton 1996). The results presented in this paper are obtained for $\alpha = 2$.

### 2.3. Stellar magnetic flux tubes

Most of the magnetic field on the surface of the Sun is observed in the form of thin flux tubes which at these heights have diameters of the order of a scale height $H_0$ (e.g., Stenflo 1978; Solanki 1993). We assume that we can

extend this well-known and commonly accepted concept of solar magnetic flux tubes to stellar flux tubes. At this point, it is important to emphasize that previous (see Saar 1996, and references therein) and recent (e.g., Rüedi et al. 1997) measurements of stellar magnetic fields provide evidence for the existence of strong magnetic fields (typical observed fields are comparable to or stronger than the equipartition field). These fields are characteristic for starspots but not for typical single magnetic flux tubes. Thus, to construct models of stellar magnetic flux tubes, we need to be guided by the results of solar observations and have to extrapolate these results to stars. Our extrapolation appears justified by the fact that the considered stars because of their surface convection zones are similar to the Sun.

As already discussed by Musielak et al. (1989, 1995), the efficiency of the generation of longitudinal tube waves increases when the "stiffness" of the tube is decreased (and the gas pressure $p$ inside the tube is increased) by decreasing the strength of the tube magnetic field (see also Ulmschneider & Musielak 1998 and Ulmschneider et al. 2001). A similar dependence on "stiffness" is found in calculations of transverse waves (Musielak & Ulmschneider 2001b). The choice of the tube field strength is thus important. Unfortunately, there are no stellar observations that would allow us to estimate the value of the plasma $\beta = 8\pi p / B^2$ for stellar magnetic flux tubes, where $p$ is the gas pressure and $B$ is the strength of the magnetic field. Similarly, there are no fully time-dependent radiation-MHD simulations of stellar magnetic flux tubes that for our range of stars would supply the value of $B$ and the amount of gas remaining in these tubes.

**Table 1.** Parameters used for constructing magnetic flux tube models, tube diameter $d_0$ (km) and magnetic field strength $B$ (G) at the stellar surface, for main-sequence stars of given spectral type, effective temperature $T_{\mathrm{eff}}$ (K), gravity $g$ (cm s$^{-2}$) and color index $B - V$.

| Star | $T_{\mathrm{eff}}$ | $\log g$ | $B - V$ | $d_0$ | $B$ |
|------|------|------|------|------|------|
| F5V | 6440 | 4.34 | 0.44 | 188 | 1410 |
| G0V | 6030 | 4.39 | 0.58 | 158 | 1570 |
| G5V | 5770 | 4.49 | 0.68 | 120 | 1740 |
| K0V | 5250 | 4.49 | 0.81 | 108 | 1850 |
| K5V | 4350 | 4.54 | 1.15 | 80 | 2370 |
| M0V | 3850 | 4.59 | 1.40 | 64 | 3260 |

As a result, we must proceed by analogy to the Sun. A tube, completely devoid of gas, but in pressure equilibrium with the outside gas would have an equipartition field strength $B = B_{\mathrm{eq}} = \sqrt{8\pi p_{\mathrm{e}}}$, where $p_{\mathrm{e}}$ is the gas pressure outside the tube. Magnetic flux tubes at the solar surface typically have field strengths of the order of $B = 1500$ G. On the other hand, taking $p_{\mathrm{e}} = 1.17 \times 10^5$ dyn cm$^{-2}$ from model C of Vernazza et al. (1981) at the height $z = 0$ where $\tau_{5000} = 1$, one gets an equipartition field strength
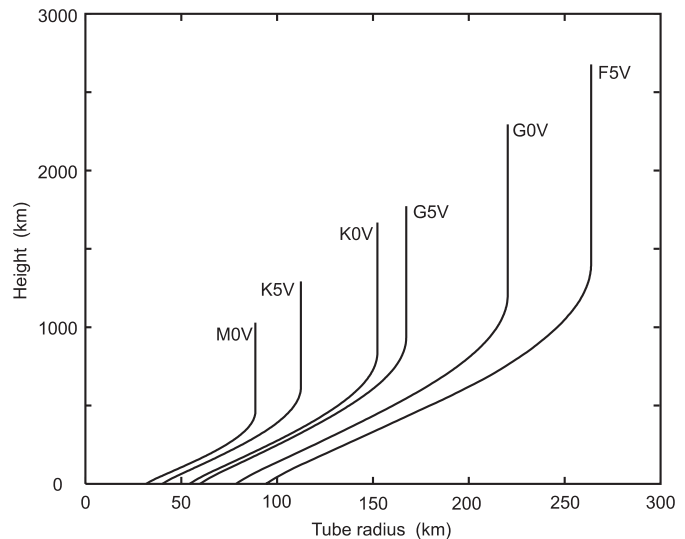


**Fig. 1.** Magnetic flux tube models for stars of different spectral types, for the case of a magnetic filling factor $f = 0.1$.

of $B_{\mathrm{eq}} = 1715$ G. We thus find a ratio $B/B_{\mathrm{eq}} = 0.875$ and consider it as typical for solar and stellar flux tubes. Although this ratio is likely to vary even on the Sun (e.g., Solanki 1993), we have adopted a field strength of $B/B_{\mathrm{eq}} = 0.85$ for all our stellar flux tubes. Since the external atmosphere can be computed using a stellar atmosphere code based on the parameters $T_{\mathrm{eff}}$, $g$ and $Z_{\mathrm{M}}$, the thin magnetic flux tube model can then be calculated using the tube diameter $d_0 = H_0$ and the magnetic field strength $B = 0.85\sqrt{8\pi p_{\mathrm{e}}}$ at the stellar surface, and by demanding magnetic flux conservation as well as horizontal pressure balance $p + B^2/(8\pi) = p_{\mathrm{e}}$ for the other heights (see Fawzy et al. 1998). Here $B^2/(8\pi)$ is the magnetic pressure and $p$ the gas pressure in the tube.

Values of $B$ and $d_0$ for a series of late-type stars are given in Table 1. The stellar parameters in this table were taken from Landolt-Börnstein (1982). Figure 1 shows magnetic flux tube models for the stars of Table 1. Note that the horizontal and vertical distance scales are very different. The bottom diameter of the tube $d_0$ is largest for the hot F5V star because of the large scale height $H_0 = \Re T_{\mathrm{eff}}/(\mu g)$, with $\Re$ the gas constant and $\mu$ the mean molecular weight at the surface. Although $d_0$ is independent of the filling factor, the amount of spreading of the tube depends on $f$. As will be shown below (see also Fig. 6), the maximum tube diameter is given by $d_{\max} = d_0\sqrt{\pi/4f}$. Figure 1 shows tube models for filling factors $f = 0.1$.

## 2.4. Wave energy fluxes for late-type stars

It is now well established that stellar chromospheres and the observed excess of chromospheric emission for late-type stars are produced by mechanical heating (e.g., Narain & Ulmschneider 1996). In our present work we explore the possibility that the mechanical heating is overwhelmingly due to acoustic and magnetic waves.

These waves are produced by turbulent flows and pressure fluctuations generated in the convection zones. Since the wave generation process depends on a high power of the velocity fluctuation (Lighthill 1952; Musielak et al. 1989; 2001a), one gets the largest contribution to the wave generation from those regions where the convective velocities are largest. Because of the rapid density decrease near the stellar surface these regions occur close to the top of the convection zones. Therefore, the first step in a wave generation computation is to obtain a reasonable representation of the flow field in the top regions of stellar convection zones.

Based on the pioneering work by Lighthill (1952) and Proudman (1952) as well as others, Stein (1967) applied their theory of acoustic sound generation from turbulent flow fields to the solar convection zone (now called Lighthill-Stein theory). Musielak et al. (1994) provided further modifications of this theory.

Our wave generation calculations are based on the assumptions that the turbulence in the convection zones can be represented by an energy spectrum

$$E'(\omega) = \int\limits_0^\infty E(k) G\left(\frac{\omega}{ku_k}\right) \mathrm{d}k, \tag{1}$$

where $E(k)$ is the spatial energy spectrum and $G$ the frequency factor derived, respectively, from the spatial and temporal correlations of velocity fluctuations in the turbulent flow field. Musielak et al. (1994) argued from recent observational and numerical work that an extended form of the Kolmogorov spectrum $E(k)$ with a modified Gaussian frequency factor $G$, that is an eKmG-spectrum is a much better representation of the turbulent flow field of the solar convection zone than previous assumptions. They proposed that $E(k)$ should be given by

$$E(k) = \begin{cases} 0 & 0 < k < ak_{\mathrm{t}} \\ b\frac{u_{\mathrm{t}}^2}{k_{\mathrm{t}}}\left(\frac{k}{k_{\mathrm{t}}}\right) & ak_{\mathrm{t}} \le k < k_{\mathrm{t}} \\ b\frac{u_{\mathrm{t}}^2}{k_{\mathrm{t}}}\left(\frac{k}{k_{\mathrm{t}}}\right)^{-5/3} & k_{\mathrm{t}} \le k \le k_{\mathrm{d}} \end{cases}, \tag{2}$$

where $a = 0.2$ and $b = 0.758$. Here $u_{\mathrm{t}}$ is the rms turbulent velocity of the flow field, $k_{\mathrm{t}} = 2\pi/H_0$ the dominant wave number with $H_0 = \Re T_{\mathrm{eff}}/(\mu g)$ being the scale height at the stellar surface and $\mu = 1.3$ the molecular weight. $k_{\mathrm{d}} = 2\pi/L$ is the wave number where the turbulent cascade ends (see Theurer et al. 1997b), for our purposes it is sufficient to take $L = H_0/100$.

For the modified Gaussian frequency factor we have

$$G\left(\frac{\omega}{ku_k}\right) = \frac{4}{\sqrt{\pi}}\frac{\omega^2}{|ku_k|^3}\mathrm{e}^{-\left(\frac{\omega}{ku_k}\right)^2} , \tag{3}$$

where

$$u_k = \left[\int\limits_k^{2k} E(k')\mathrm{d}k'\right]^{1/2} . \tag{4}$$

According to Musielak et al. (1994), the forms of $E(k)$ and $G$ are chosen because in the former the main energy

carrying eddies have vertical sizes of roughly one scale height $H_0$ and the maximum contribution to $G$ is from bubbles which have just traveled a distance equal to their own diameter.

Using a stellar convection zone model based on the values of $\alpha$, $T_{\mathrm{eff}}$, $g$ and solar metallicity, $Z_{\mathrm{M}}$, *acoustic fluxes* and *acoustic spectra* are computed on basis of this eKmG turbulent energy spectrum following Musielak et al. (1994) and Ulmschneider et al. (1996). For these computations we assume that $u_{\mathrm{t}} = v_{\mathrm{conv}}$, where $v_{\mathrm{conv}}$ is the height-dependent convective velocity which is obtained from a convection zone model. The total acoustic fluxes computed this way for a series of main-sequence stars are shown in Table 2.

For the computation of the magnetic wave generation, thin magnetic flux-tube models are constructed as discussed above. These tubes are perturbed by the turbulent motions existing in the convection zone regions outside the tube. Here pressure fluctuations give rise to *longitudinal tube waves* and velocity fluctuations to *transverse tube waves*.

There are two approaches to these magnetic wave generation computations, an *analytical approach* similar to the Lighthill-Stein theory, and a *numerical approach*. The analytical approach by Musielak et al. (1989, 1995) for longitudinal and by Musielak & Ulmschneider (2001a,b) for transverse waves gives results which are valid for small amplitude (linear) fluctuations. As this approach neglects the occasionally large amplitude fluctuations we believe that it provides lower estimates for the wave fluxes. But the advantage of this method is that it allows to take into account correlation effects resulting from a simultaneous squeezing and shaking of the flux tube along its entire length.

The numerical approach consists of applying time-dependent squeezing and shaking at a single specified height (for which we take the stellar surface) to the flux tube. These squeezings and shakings are assumed to be caused by external velocity fluctuations, which are modeled by the superposition of a large number of partial waves of frequencies $\omega_n$

$$v_{\mathrm{x}}(t) = \sum_{n=1}^N u_n \sin(\omega_n t + \varphi_n), \tag{5}$$

where $u_n$ is the velocity amplitude and $\varphi_n = 2\pi r_n$ is an arbitrary but constant phase angle with $r_n$ a random number in the interval [0, 1] (Ulmschneider & Musielak 1998). The velocity amplitudes $u_n$ are related to $v_{\mathrm{x}}$ and the rms turbulent velocity fluctuation, $u_{\mathrm{t}}$, by

$$\overline{v_{\mathrm{x}}^2} = u_{\mathrm{t}}^2 = \frac{1}{2}\sum_{n=1}^N u_n^2 , \tag{6}$$

where

$$u_n = \sqrt{\frac{4}{3}E'(\omega_n)\Delta\omega} , \tag{7}$$

and $E'$ is given by Eq. (1). Here again an eKmG turbulent energy spectrum is taken.

To generate transverse waves, $v_x$ is applied as boundary condition of our time-dependent wave code at the excitation height at the stellar surface (Huang et al. 1995), while

$$v_\parallel = \frac{\beta}{2/\gamma + \beta} \frac{3\rho_e(v_x^2 - u_t^2)}{\rho_0 c_{T0}} . \tag{8}$$

is applied to generate longitudinal waves (Ulmschneider et al. 2001). Here $\rho_0$, $p_0$, $c_{T0}$ are the density, gas pressure and wave speed inside the tube, $\beta = 8\pi p_0/B^2$, $\gamma$ is the ratio of specific heats and $\rho_e$ is the external density all at the excitation height. Note that while in our analytical approach $u_t$ is a height-dependent quantity, the single value $u_t$ at the excitation height in the numerical approach is taken to be one half of the maximum convective velocity $v_{conv}$ which occurs in the convection zone model.

This way, for given values of $\alpha$, $T_{eff}$, $g$ and $B = 0.85B_{eq}$, more realistic energy fluxes and spectra carried by nonlinear longitudinal waves (Ulmschneider & Musielak 1998; Ulmschneider et al. 2001) and nonlinear transverse waves (Huang et al. 1995) have been computed for main-sequence stars. Note that in these computations, due to our assumption that the flux-tubes at the stellar surface have a diameter $d_0 = H_0$ and as $B = 0.85\sqrt{8\pi p_e}$, the magnetic wave energy generated in an individual flux tube does not depend on the filling factor $f$. However, as a larger filling factor implies more magnetic flux, the number of flux tubes on the star and thus the total generated magnetic wave energy increases with the filling factor. As shown below, the filling factor also affects the magnetic wave heating because with increasing $f$, the space available for the spreading tube decreases.

The waves generated in the tube represent a mixture of propagating (with frequencies higher than the Defouw frequency, $\omega_D$) and non-propagating (with frequencies lower than $\omega_D$) longitudinal tube waves. The reason for this is that both the turbulent energy spectrum and the frequency factor of the fluid motions in the nonmagnetic flow field outside the tube are independent of the cutoff frequency of the waves inside the tube. Therefore, the total velocity perturbations $v_\parallel$ generated in the tube by the outside pressure perturbations depend on frequencies both above and below $\omega_D$. As we are only interested in propagating waves, the non-propagating wave perturbations have to be removed by using Fourier techniques. To compute the upward propagating wave flux we follow Ulmschneider et al. (2001).

### 2.5. Wave spectra and monochromatic waves

The longitudinal wave energy spectra calculated using the method of Ulmschneider et al. (2001) for the main-sequence stars of Table 2 are shown in Fig. 2. The table also displays the computed total upward propagating wave energy fluxes $F_L$ obtained by using the numerical approach and taking field strengths $B = 0.85B_{eq}$. It is
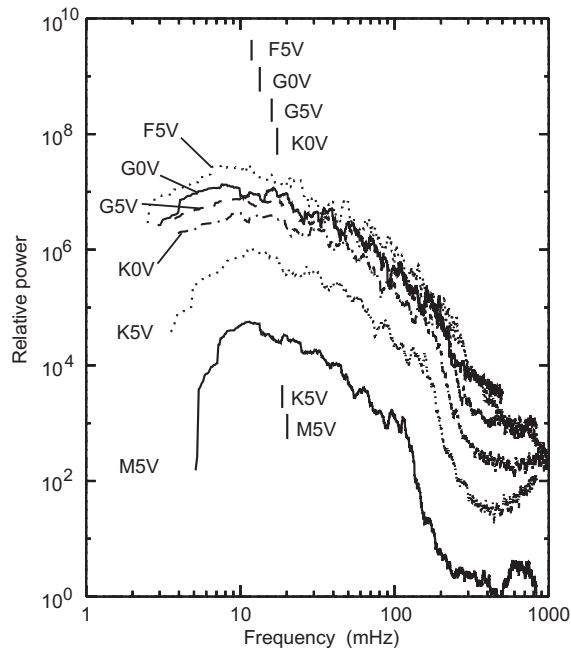


**Fig. 2.** Power spectra of the generated longitudinal tube waves for different stars, assuming a magnetic field strength $B = 0.85B_{eq}$. Frequencies taken for monochromatic wave calculations are marked.

seen that the spectra decrease in magnitude in proportion to $F_L$ and that the maxima of the spectra shift slightly towards higher frequency for later spectral types.

Since our current calculations of the wave propagation (see Buchholz et al. 1998; Cuntz et al. 1999) are performed by using *monochromatic waves* in which we picture the total wave flux $F_L$ as carried by a longitudinal wave with period $P_L$, we now discuss the process by which we select this wave period. That monochromatic waves are used in our present work instead of the entire generated wave spectrum (see work by Theurer et al. 1997a,b, for the Sun) is due to the fact that a radiation-hydrodynamic wave calculation for a full spectrum requires a code which is able to treat the time-dependent hydrogen ionization by solving the time-dependent rate equations for the hydrogen atomic levels. This is because the low frequency components of the wave spectrum produce strong solitary shocks which cannot be accurately handled by using our present methods. Since these occasionally occurring solitary shocks are a peripheral feature of the chromospheric heating picture (Kalkofen et al. 1999; Theurer et al. 1997b) we think that by avoiding these solitary shocks a reasonably accurate chromospheric heating can be achieved with our present methods in which we use a non-ionizing wave code and monochromatic waves. This view is also warranted because we use the entire available generated wave energy for the heating of the outer stellar atmosphere, and the wave code only specifies how this energy is distributed over height.

For the monochromatic wave calculation we have selected wave periods $P_L$ which correspond to the maximum of the (smoothed) longitudinal wave spectrum (actually

**Table 2.** Total propagating longitudinal tube wave fluxes $F_{\rm L}$ and acoustic fluxes $F_{\rm A}$ (erg cm$^{-2}$ s$^{-1}$) for main-sequence stars of given spectral type, $T_{\rm eff}$ (K) and gravity (cm s$^{-2}$). Also given are the longitudinal $P_{\rm L}$ (s) and acoustic $P_{\rm A}$ (s) wave periods used for monochromatic wave calculations.

| Star | $T_{\rm eff}$ | $\log g$ | $F_{\rm L}$ | $P_{\rm L}$ | $F_{\rm A}$ | $P_{\rm A}$ |
|------|------|------|------|------|------|------|
| F5V | 6440 | 4.34 | $1.1 \times 10^9$ | 85 | $6.7 \times 10^8$ | 55 |
| G0V | 6030 | 4.39 | $8.8 \times 10^8$ | 75 | $3.2 \times 10^8$ | 46 |
| G5V | 5770 | 4.49 | $5.6 \times 10^8$ | 63 | $1.7 \times 10^8$ | 42 |
| K0V | 5250 | 4.49 | $3.8 \times 10^8$ | 58 | $5.2 \times 10^7$ | 38 |
| K5V | 4350 | 4.54 | $1.1 \times 10^8$ | 54 | $3.8 \times 10^6$ | 34 |
| M0V | 3850 | 4.59 | $2.0 \times 10^7$ | 50 | $3.6 \times 10^5$ | 31 |

taking values at the high-frequency side of this maximum). The values are given in Table 2 and are also displayed in Fig. 2 in relation to the wave spectra. In a similar way we evaluate the acoustic energy generation by following Ulmschneider et al. (1996). The generated total acoustic wave fluxes $F_{\rm A}$ and monochromatic wave periods $P_{\rm A}$ are also displayed in Table 2.

# 3. Initial atmosphere models and the wave propagation

## 3.1. Piston boundary condition

To compute the propagation of acoustic waves we solve the one-dimensional, time-dependent hydrodynamic equations consisting of the continuity, momentum, and energy equations utilizing the modified method of characteristics, as described in our previous work (Ulmschneider et al. 1977; Ulmschneider & Kalkofen 1978; Schmitz et al. 1985; Ulmschneider et al. 1987; Rammacher & Ulmschneider 1992; Buchholz et al. 1998).

At the bottom of the external atmosphere at optical depth $\tau_{5000} = 1$, monochromatic sinusoidal acoustic waves are introduced by specifying the piston velocities $v(t) = -v_{\rm A} \sin(2\pi t/P_{\rm A})$, where $P_{\rm A}$ is the period and $v_{\rm A} = \sqrt{2F_{\rm A}/(\rho_0 c_0)}$ is the velocity amplitude determined from the initial acoustic wave energy flux $F_{\rm A}$, which together with $P_{\rm A}$ is given in Table 2. Here $\rho_0$ is the density and $c_0$ the sound speed at the bottom of the atmosphere model. The specified gravity $g$ and effective temperature $T_{\rm eff}$ of the star enters as a term in the hydrodynamic equations and as radiative boundary condition (specifying the outgoing radiative intensity) at the bottom of the atmosphere, respectively. The propagation of the waves is calculated numerically to the point of shock formation and beyond. The shocks are treated as discontinuities by solving the Rankine-Hugoniot equations, and are permitted to grow to arbitrary strength. At the top of the atmosphere we use a transmitting boundary condition. Note that in order to avoid a violent initial transient behavior the velocity amplitudes in all calculations are slowly increased from zero until after 9 wave periods they attain

their full specified value. To achieve dynamical equilibrium the acoustic wave calculations are typically continued for about 43 wave periods.

The computation of longitudinal waves is very similar to that of acoustic waves and is fully implemented in our hydrodynamic wave code for acoustic waves (see Herbold et al. 1985; Rammacher & Ulmschneider 1989; Fawzy et al. 1998). The set of MHD equations is simplified by taking into account the thin flux tube approximation and is solved by using the modified method of characteristics (see also Cuntz et al. 1999). The monochromatic longitudinal wave is introduced at the bottom of the magnetic flux tube model by specifying the piston velocities $v(t) = -v_{\rm L} \sin(2\pi t/P_{\rm L})$, where $P_{\rm L}$ is the period and $v_{\rm L} = \sqrt{2F_{\rm L}/(\rho_0 c_{\rm T0})}$ the velocity amplitude determined from the initial longitudinal wave energy flux $F_{\rm L}$, which together with $P_{\rm L}$ is given in Table 2. Here $c_{\rm T0}$ is the tube speed at the bottom of the tube model. The shocks are computed by using magnetic versions of the Hugoniot relations (see Herbold et al. 1995). Again we assume a transmitting boundary condition at the top. Here also the wave amplitude is slowly increased over 40 wave periods, and the total calculation typically lasts for about 53 wave periods.

For the computation of the magnetic waves, we have to take into account the fact that the longitudinal tube waves heat the medium directly by shock dissipation, however, the transverse tube waves require nonlinear mode-coupling to longitudinal waves (Ulmschneider et al. 1991) to dissipate their carried energy. Although the propagation of both transverse and longitudinal waves could be simulated in principle by performing a time-dependent computation (see Ulmschneider et al. 1991; Zhugzhda et al. 1995), we defer such computations to future work because in these codes the radiation treatments are not yet fully implemented and particularly because the questions about leakage of transverse wave energy away from the flux tube (Ziegler & Ulmschneider 1997; Huang et al. 1999) is not yet sufficiently understood. Note that the work of Zhugzhda et al. (1995) has shown that particularly at shock formation, very strong mode-coupling occurs because despite of the different propagation speeds of the two wave types, there are no separate transverse and longitudinal shocks. One rather finds that the kink shocks and longitudinal shocks coincide and propagate with a common speed.

To simplify the situation, we thus assume that a specified fraction of the transverse wave flux becomes available as longitudinal wave flux and compute the propagation and shock formation of the longitudinal wave only. Since we found that the generated transverse wave energy is roughly by a factor of 30 greater than the longitudinal wave energy (Huang et al. 1995; Musielak & Ulmschneider 2001a,b) we simulate the mode-coupling by increasing the generated longitudinal wave fluxes given in Table 2 by an assumed wave flux multiplication factor $M$ for which we take values between 1 and 5, that is, by actually using fluxes $F = MF_{\rm L}$.
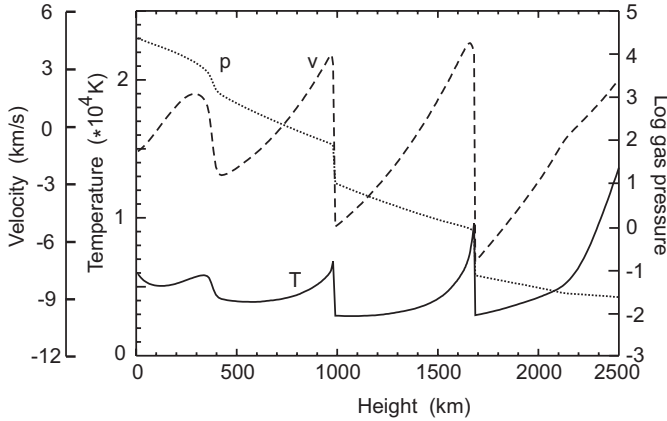
**Fig. 3.** Snapshot of temperature $T$ (K), velocity $v$ (km s$^{-1}$) and logarithm of the gas pressure $p$ (dyn/cm$^2$) as a function of height $z$ (km) in a magnetic flux tube on an F5V star covered by magnetic fields with a filling factor $f = 0.1$. For fluxes $F_L$ with a multiplication factor $M = 0.5$ at time $t = 2000$ s.
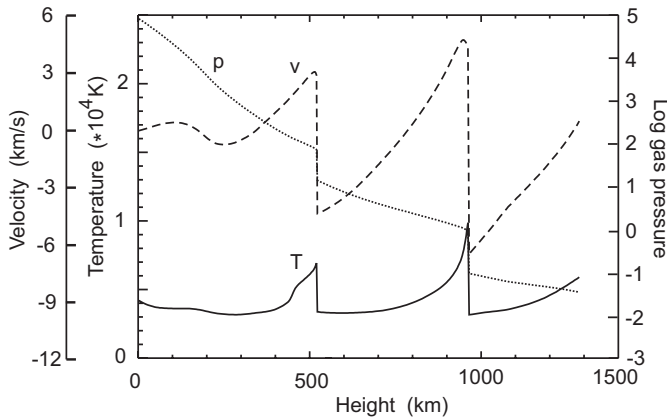


**Fig. 4.** The same as in Fig. 3 but for a K5V star.

Figures 3 and 4 show snapshots of magnetic tube wave calculations at times $t = 2000$ s for the F5V star and the K5V star. Here about 30 shocks have already transmitted at the top boundaries and the state of dynamical equilibrium has set in. Similar calculations were performed for the acoustic waves. Note also that contrary to our acoustic wave calculations (Buchholz et al. 1998, Fig. 1), Figs. 3 and 4 do not show the limiting shock strength behavior by which the temperature-jumps at the shocks become similar as soon as the waves have grown into a fully developed sawtooth wave. This means that the behavior of the temperature in the tubes models depends strongly on the spreading, that is, on the growth of the tube diameter with height. At greater height, where the tubes attain a constant cross-section, the limiting shock strength behavior is expected to reappear (see Fawzy et al. 1998).

### 3.2. Initial atmosphere models

With time-dependent wave codes one usually starts with initial atmosphere models which are constructed by employing temperature correction methods (Cuntz et al. 1999) and using the same emitters as for the wave code. This is because in absence of piston motions, these models then do not show major velocity and temperature fluctuations. However, it has to be noted, that because of the absence of mechanical heating, these initial models are quite unrealistic, as due to the small scale height, most of the mass is concentrated at the bottom of the models. To distribute this mass realistically over height, the wave heating must act for a considerable time, until a dynamical equilibrium state is reached and switch-on effects have died out.

The initial atmosphere models are constructed by specifying the stellar parameters effective temperature $T_{\rm eff}$, gravity $g$, and magnetic filling factor $f$ at the stellar surface. At first a model in radiative and hydrostatic equilibrium of the non-magnetic external atmosphere is generated by using temperature correction methods to ensure that the specified radiation flux $\sigma T_{\rm eff}^4$ is correctly reproduced. Subsequently in this external atmosphere a magnetic flux tube model is embedded with a magnetic field strength of $B = 0.85 B_{\rm eq}$ at the stellar surface and a tube diameter of $d_0 = H_0$ at that height. The values for $d_0$ and $B$ for the chosen stars are given in Table 1. The shape of this flux tube is determined by magnetic flux conservation and horizontal pressure balance and after first spreading exponentially is constrained by the magnetic filling factor $f$ (see Fig. 1, for details see Fawzy et al. 1998). The temperature in the flux tube is again determined by employing temperature correction methods. It typically is close to the external temperature. Figure 5 shows initial temperature distribution of such tube models constructed in hydrostatic and radiative equilibrium, that is, in absence of mechanical heating.

A persistent feature of these models, seen particularly for the M0V star, but occurring for all stars, is that the temperature after reaching a minimum, increases again in outward direction without mechanical heating. This is a purely NLTE radiative equilibrium effect due to H$^-$ known as Cayrel effect (Cayrel 1963, 1964) which is partially counteracted by our Ca II and Mg II line cooling. More realistic models include a large amount of additional emitters such that this purely radiative temperature rise may be lower or nonexistant.

## 4. Chromospheric emission and radiation flux

### 4.1. The chromospheric emitters

For the treatment of the radiative losses (and gains) required for the energy equation we take the H$^-$ continuum as well as the Ca II, Mg II and Fe II lines into account by solving the radiative transfer equations and the statistical equilibrium equations for NLTE populations (Ulmschneider & Kalkofen 1978; Ulmschneider et al. 1987). The ionization of hydrogen is taken into account as far as the electron density is concerned which enters the line-radiation. For this, we assume that the hydrogen departure coefficients by Hartmann & McGregor (1980)
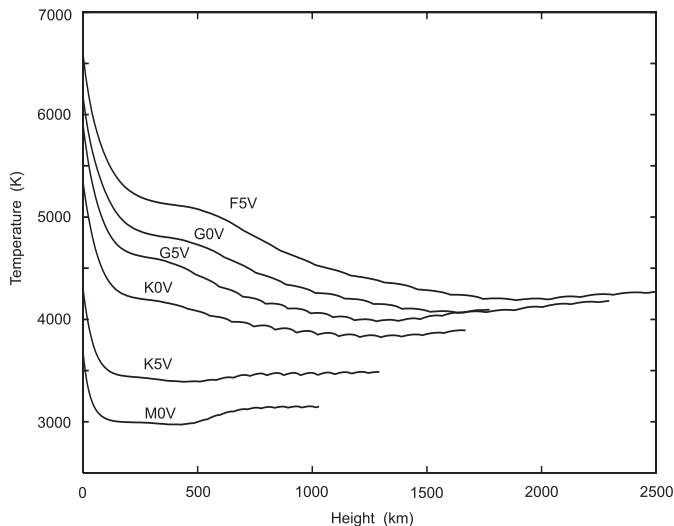
**Fig. 5.** Initial temperature distributions in magnetic flux tubes covering the main sequence stars of Table 2 with a magnetic filling factor $f = 0.1$.



**Fig. 6.** A side view of rows of magnetic flux tubes for two stars with different magnetic filling factors; a star with low filling factor (Sun, $f = 0.015$, left) and high filling factor ($f = 0.4$, right), dashed arrows show the ray paths inclined by the angle $\phi$ with respect to the vertical.

can be used. As we are only concerned with the chromosphere up to the height of the formation of the Mg II h+k line cores, we have not included the effects of the hydrogen ionization on the composition of the medium and assume that we can deal with an non-ionized gas of mean molecular weight $\mu = 1.3$.

The correct treatment of the radiative losses in the chromospheric emission lines, required for the computation of the energy conservation in the hydrodynamic equations, necessitates the use of partial redistribution PRD (e.g., Ulmschneider 1994) because the line wings are formed by coherent scattering and only the line cores contribute to the radiative energy loss. However, a line treatment implementing PRD (Ulmschneider 1994) is mathematically complex and leads to excessive computation times that cannot be tolerated in time-dependent wave calculations. We thus follow Hünerth & Ulmschneider (1995) who employed the so-called pseudo-PRD, which artificially removes the damping wings from the lines by multiplying the damping parameter $a$ in the Voigt function by a factor $1/100$ and computes the line assuming complete frequency redistribution CRD. Simulations of solar Mg II line cooling show that pseudo-PRD works very well (Hünerth & Ulmschneider 1995).

In order to achieve rapid progress of the time-dependent calculations, we do not want to compute the total chromospheric radiation losses by employing complicated multilevel atomic models of Ca II, Mg II and Fe II. We rather approximate the ions by a two level atom treated in pseudo-PRD and multiply the single line emission by factors to take into account the other lines of the given ion. We thus multiply our Mg II k-line computation by a factor 2 to also account for the Mg II h-line and the Ca II K-line computation by a factor of 5 to take into account the H-line and the three IRT lines. We found that the Fe II emission can also be crudely taken into
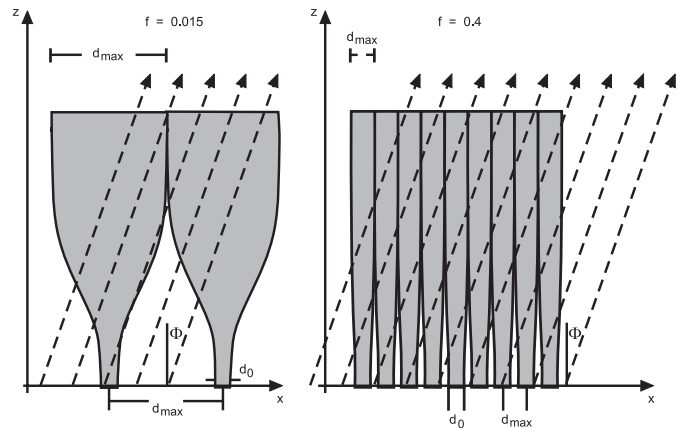
account by simply doubling the Ca II losses. In our computations we therefore multiply the Ca II K-line pseudo-PRD losses by a factor 10. For the computations of the single lines we use a revised operator splitting method (Buchholz et al. 1994) which allows for the proper handling of shocks. We use 19 frequency points for H$^-$ and 29 frequency points each for the Mg II K and Ca II K lines.

In our treatment of the radiation in the magnetic flux-tube models, we assume that for H$^-$ the tubes are optically thin and, therefore, the mean intensity is given as height-dependent function from an external acoustic wave computation. The NLTE source function of H$^-$ in the tubes can then be determined locally and the H$^-$ losses become a local function of temperature and density. For the chromospheric lines, however, we assume that the optical depth across the tube is so large that we can use a similar two beam radiation treatment as employed for the outside medium.

It has to be noted that these radiation treatments apply to our time-dependent wave computations only. After the completion of the wave calculation, individual snapshots of the wave can be taken to compute more accurate radiation properties using extensive multilevel atom models and applying the full PRD treatment for the involved lines. This way the emergent radiation fluxes are determined, and the accuracy of our rapid approximation to compute the total chromospheric radiation losses can be evaluated.

### 4.2. Multi-ray radiative transfer

Once the wave computation is completed, we compute the average emerging radiation flux from the stars in the Mg II h+k and Ca II H+K lines. Figure 6 shows the magnetic field geometry of two stellar regions of different filling factor $f$. It is seen that the individual flux tubes (indicated gray) which at the stellar surface have a diameter of $d_0$ spread with height $z$ until they meet the neighboring flux

tubes, and with a maximum diameter $d_{max}$ fill out the entire available space. In horizontal direction $x$ the next flux tube lies a distance $d_{max}$ away. Assuming a circular cross-section of the flux tube at the stellar surface, the filling factor is given by $f = \pi d_0^2/(4d_{max}^2)$ which permits to write the maximum diameter of the tube as $d_{max} = d_0\sqrt{\pi/4f}$. The figure shows that $d_{max}$ narrows with increasing filling factor as at the stellar surface the tube diameter is assumed to be given by $d_0 = H_0$, independent of $f$. Thus $d_0$ will be the same for stars with similar $T_{eff}$, $g$ and $Z_M$, and the figure shows the situation when only $f$ is varied. Although in Fig. 6 for $f = 0.4$ the magnetic area appears to be larger than the non-magnetic area, the diameter of the region between the circular tubes is still greater than $d_0$.

Because the number of flux tubes increases when $f$ is increased, one injects more magnetic wave flux into the outer atmosphere, and as the heating in narrower flux tubes is more intense (Fawzy et al. 1998), the two cases shown in Fig. 6 will have very different magnetic wave heating. In addition, one has acoustic heating in the medium outside the magnetic regions.

Recalling that we perform time-dependent wave calculations both inside and outside the magnetic tubes, let us now consider the radiation emitted from this two-component tube forest model. For the outside medium, we select a wave phase from an acoustic wave calculation which is close in emission to the average of all phases. Since the magnetic waves propagate independently from one another in each tube, we select four different wave phases (spaced equally in time) from a magnetic wave computation along a single flux tube and place them in the two-dimensional surface region in four adjacent tubes. This way, the stellar surface is assumed to be completely covered by repeating sequences of blocks of four fluxtubes with different wave phases.

Emanating from the two-dimensional surface region at origin points, equidistantly spaced ray paths of sufficient resolution are assumed to emerge (Fig. 6). They penetrate the magnetic and non-magnetic regions and the source function (computed assuming PRD) is integrated along the ray paths emanating at a constant angle $\phi$ with respect to the vertical. For more details of this procedure see Rammacher & Ulmschneider (1989) and Ulmschneider (1994). The total emerging line intensity profile is the average over the individual rays.

In order to sample all possible situations, 600 origin points are selected. For the emerging fluxes five angles (at $\cos\phi = 0.9$, 0.7, 0.5, 0.3, and 0.1) were taken to ensure that all angles equally contribute to the integrated flux. However, it was found that it is sufficiently accurate to take the single oblique angle $\cos\phi = 1/\sqrt{3}$, which we also use for our two-beam radiative transfer calculations in the wave computation.

The Mg II k and Ca II K emission lines and frequency-dependent source functions are computed for each wave phase, height and selected ray angle assuming PRD by using a two-level atom description and employing the

operator splitting method described by Ulmschneider (1994). We use 29 frequency points, distributed within $\pm 10$ Å of line center. Since the $K_1$ minima and the $K_2$ emission peaks in the models are always located within $\pm 0.3$ Å from line center, 21 of these frequency points are concentrated in this core range. For the individual wave phases these core frequency grid is shifted by small fractions $\delta\lambda$ of the grid distance $\Delta\lambda$ to capture the sharp emission peaks. Examples of such line profiles are seen below in Figs. 7 and 8. The source functions of the different mhd wave phases and the external acoustic wave phase are then interpolated onto a common frequency grid of much higher resolution (47 frequency points) for the multi-ray intensity integration through the tube rows.

### 4.3. Integrated line profiles and emergent emission fluxes

Once the wave calculations are completed, we use the above discussed multi-ray method to compute the lines of Ca II K and Mg II k which emerge from our two-component flux-tube forest, assuming PRD. As discussed above, we select (four) different phases from the longitudinal wave calculation together with an average phase from the acoustic wave computation. Integrating the line profiles $I^+(\Delta\lambda)$ over wavelength $\Delta\lambda$ in the line core (between $\pm 3$ Å), the K and k-line fluxes $F = 2\pi\mu I^+$ are computed and after multiplying with 2 to take into account the other line of the doublet the total emerging emission fluxes of the Ca II H+K and Mg II h+k lines are evaluated. Here $\mu = 1/\sqrt{3}$ is the angle cosine. For the Ca II lines we subsequently subtract the fluxes due to the photospheric background by generating line intensities similarly as for the wave calculations, however now for the initial tube and external atmospheres. Since the photospheric background is not important for the Mg II lines, we did not apply further corrections to those flux values.

## 5. Simulated theoretical line profiles and emission fluxes

As an example Fig. 7 shows (solid line) the emerging core intensities from an acoustic wave calculation of the F5V star using the flux $F_A$ and period $P_A$ given in Table 2. This calculation was carried out until after the time 2493 s, 40 shocks have transmitted. The figure shows 4 subsequent wave phases separated by 14 s, starting with 2493 s. Also shown (dashed line) is the intensity profile of the external initial atmosphere similar to Fig. 5. Surprisingly at first sight, this latter atmosphere in radiative and hydrostatic equilibrium, that is, *without mechanical heating*, does also show emission peaks. As discussed above these peaks are produced by the Cayrel effect and are most likely an artifact of our restricted set of emitters. For the Ca II H+K lines from the F5V star, we find a total flux of $1.8 \times 10^6$, for the total flux corrected for the photospheric background we obtain $8.7 \times 10^5$ and for the total photospheric background $8.9 \times 10^5$ erg cm$^{-2}$ s$^{-1}$. To compute
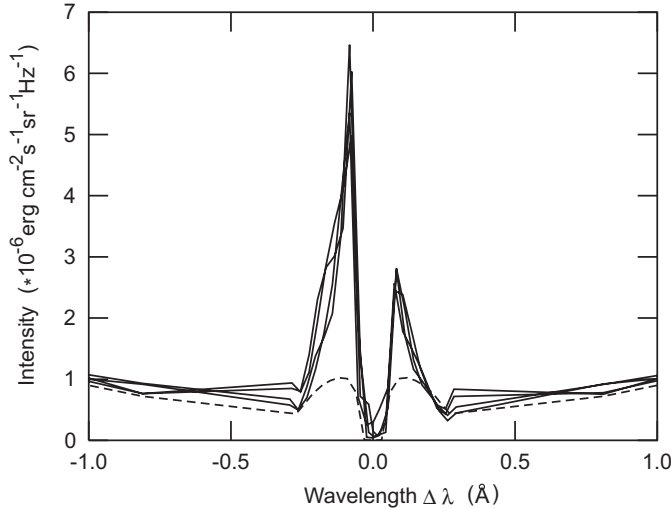
**Fig. 7.** Ca II K line intensities of four phases (solid) of an acoustic wave calculation for the F5V star given in Table 2. Also shown is the intensity (dashed) of the initial undisturbed atmosphere.



**Fig. 8.** Mg II k line intensity profiles for different angles $\phi$ for the G5V star with a magnetic filling factor $f = 0.2$ and multiplication factor $M = 0.5$.

these total fluxes the individual fluxes of the 4 phases were averaged.

The influence of the aspect angle on the emergent intensity from the flux tube forest is shown in Fig. 8 for a G5V star with a magnetic filling factor $f = 0.4$ using the data given in Table 2 and increasing the longitudinal flux $F_L$ with a multiplication factor $M = 5$. The Mg II k-line profiles are for different angles $\phi$ (in degrees) from the vertical. It is seen that for small $\phi$ there is a large asymmetry between the violet and red emission peaks which can be attributed to the strong velocity-temperature correlation in the post-shock regions combined with the removal of the violet opacity by Doppler shift in the front-shock regions for acoustic and longitudinal waves traveling in vertical direction. This effect has already been discussed in detail by Rammacher & Ulmschneider (1992). It is seen that this correlation is lost when one looks onto the tube forest from the side when $\phi$ is large. Here the velocities are perpendicular to the line of sight and thus close to zero, and the post-shock temperatures produce the symmetric emission cores.

A comparison of emission cores of the Ca II K and Mg II k lines for different stars, both for pure acoustic waves (filling factor $f = 0.0$) and magnetic waves (filling factor $f = 0.4$ and $M = 5$), are shown in Fig. 9. These profiles, which represent momentary wave phases in a magnetic flux tube and in the external non-magnetic atmosphere, clearly show that magnetic wave heating strongly enhances the chromospheric emission relative to pure acoustic heating. Also seen is the decrease of the emission towards later spectral type which is due to a decrease of the acoustic and longitudinal wave fluxes. This is ultimately caused by the decreasing convective velocities in these stars.

As we are mainly interested in the chromospheric emission fluxes and want to reduce the large computation time
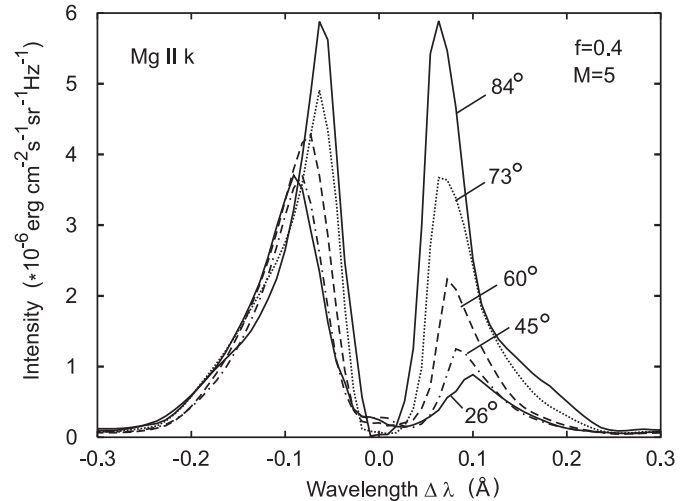
for our full PRD line profile calculations, we used only 29 frequency points. A careful comparison with observed profiles will require theoretical profiles based on a more extended frequency grid, employing more wave phases and particularly using an acoustic wave spectrum instead of monochromatic waves. Such investigations are presently undertaken and will be published separately. In Fig. 9 the displayed asymmetries of the red and violet emission peaks appear to be too large compared to observed ones, which may be due to our use of monochromatic waves, although large asymmetries have been observed (see Pasquini et al. 1988).

## 6. Conclusions

We have outlined a *theoretical method based completely on first principles* to construct theoretical chromosphere models and simulate chromospheric emission fluxes in the Ca II H+K and Mg II h+k lines for late-type main sequence stars. The method requires specifying only the four basic stellar parameters: effective temperature $T_{eff}$, gravity $g$, metallicity $Z_M$ (only solar-like population I metal abundances are considered in this paper), and magnetic filling factor, $f$, at the stellar surface. With these four parameters, which uniquely identify a star, we construct convection zone models and models of the magnetic flux tube forest which homogeneously covers the stellar surface. Here we assume that the magnetic field occurs mainly in the form of thin flux tubes, which at the stellar surface have diameters equal to the local scale height. The magnetic field strength at this height is assumed to be given by a fixed fraction of the equipartition field strength, which is determined by the external gas pressure.

Using the Lighthill-Stein theory for the acoustic waves and a numerical method for the magnetic tube waves, we have calculated acoustic, longitudinal and transverse tube wave fluxes and determined wave periods. To take into
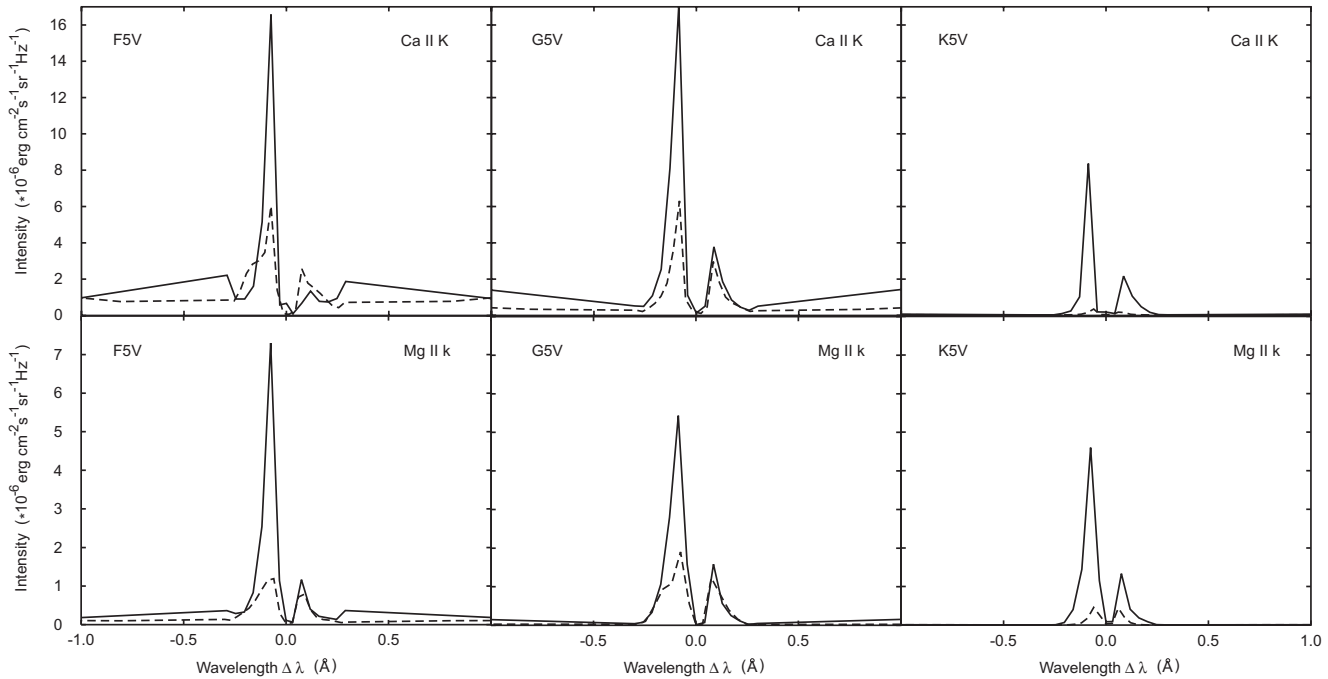
**Fig. 9.** Emission cores of the Ca II K and Mg II k lines for different stars both for pure acoustic waves (filling factor $f = 0.0$, dashed) and magnetic waves (filling factor $f = 0.4$ and $M = 5$, solid).

account transverse waves, the longitudinal wave fluxes are increased by a factor $M$, which for realistic cases will be around $M = 5$. The waves are allowed to propagate and heat both components of these models by shock dissipation. The time-dependent energy balance between the amount of dissipated wave energy and the most prominent chromospheric radiative losses is calculated at each height in stellar atmospheres. For the obtained models, the emerging radiative fluxes in the Ca II and Mg II lines are computed by using a newly developed multi-ray radiative transfer method. In the second paper of this series, we shall use the presented approach to determine the theoretical range of chromospheric activity in late-type stars and compare it with observations. This will allow us to address an important (and currently unsolved) problem of the role played by acoustic and magnetic wave energy in heating of different regions of stellar atmospheres.

## References

Bohn, H. U. 1984, A&A, 136, 338

Buchholz, B., Ulmschneider, P., & Cuntz, M. 1998, ApJ, 494, 700

Cayrel, R. 1963, CR Acad. Sci. Paris, 257, 3309

Cayrel, R. 1964, Smiths. Astrophys. Obs. Spec. Rept., 167, 169

Cuntz, M., Rammacher, W., Ulmschneider, P., Musielak, Z. E., & Saar, S. H. 1999, ApJ 522, 1053

Fawzy, D. E., Ulmschneider, P., & Cuntz, M. 1998, A&A, 336, 1029

Hartmann, L., & MacGregor, K. B. 1980, ApJ, 242, 260; 1996, AJ, 111, 439

Herbold, G., Ulmschneider, P., Spruit, H. C., & Rosner, R. 1985, A&A, 145, 157

Huang, P., Musielak, Z. E., & Ulmschneider, P. 1995, A&A, 279, 579

Huang, P., Musielak, Z. E., & Ulmschneider, P. 1999, A&A, 342, 300

Hünerth, G., & Ulmschneider, P. 1995, A&A, 293, 161

Hünsch, M., & Schröder, K.-P. 1997, A&A, 309, L51

Kalkofen, W., Ulmschneider, P., & Avrett, E. H. 1999, ApJ, 521, L141

Landolt-Börnstein 1982, New Ser. 453, ed. K.-H. Hellwege, Group VI, vol. 2b (Springer, Berlin), 31

Lighthill, M. J. 1952, Proc. Roy. Soc. London A, 211, 564

Linsky, J. L. 1980, ARA&A, 18, 439

Musielak, Z. E., Rosner, R., & Ulmschneider, P. 1989, ApJ, 337, 470

Musielak, Z. E., Rosner R., Gail, H. P., & Ulmschneider, P. 1995, ApJ, 448, 865

Musielak, Z. E., Rosner R., Stein, R. F., & Ulmschneider P. 1994, ApJ, 423, 474

Musielak, Z. E., & Ulmschneider, P. 2001a, A&A, 370, 541

Musielak, Z. E., & Ulmschneider, P. 2001b, A&A, 386, 606

Narain, U., & Ulmschneider, P. 1996, Space Sci. Rev., 75, 453

Noyes, R. W., Hartmann, L. W., Baliunas, S. L., Duncan, D. K., & Vaughan, A. H. 1984, ApJ, 279, 763

Pasquini, L., Pallavicini, R., & Pakull, M. 1988, A&A, 191, 253

Proudman, I. 1952, Proc. Roy. Soc. London, A214, 119

Rammacher, W., & Ulmschneider, P. 1989, in Solar & Stellar Granulation, ed. R. J. Rutten, & G. Severino (Kluwer Academic Publ.), 589

Rammacher, W., & Ulmschneider, P. 1992, A&A, 253, 586

Rüedi, I., Solanki, S. K., Mathys G., & Saar, S. H. 1997, A&A, 318, 429

Saar, S. H. 1996, in Stellar Surface Structure, ed. K. Strassmeier, & J. L. Linsky (Kluwer), IAU Symp. 176 (Academic Publ.), 237

Schmitz, F., Ulmschneider, P. & Kalkofen, W. 1985, A&A, 148, 217

Schrijver, C. J. 1987, A&A, 172, 111

Schröder, K.-P., & Eggleton, P.P. 1996, Rev. Mod. Astr., 9, 221

Solanki, S. K., 1993, Space Sci. Rev., 63, 1

Steffen, M. 1993, Habil. Thesis, Univ. Kiel, Germany

Stein, R. F. 1967, Solar Phys., 2, 385

Stenflo, J. O. 1978, Rep. Prog. Phys., 41, 865

Stępień K. 1994, A&A, 292, 191

Strassmeier, K. G., Handler, G., Paunzen, E., & Rauth M. 1994, A&A, 281, 855

Theurer, J. 1993, Diplome Thesis, Univ. Heidelberg, Germany

Theurer, J., Ulmschneider, P., & Cuntz, M. 1997a, A&A, 324, 587

Theurer, J., Ulmschneider, P., & Kalkofen, W. 1997b, A&A, 324, 717

Trampedach, R., Christensen-Dalsgaard, J., Nordlund, A., & Stein, R. F. 1997, in Solar Convection and Oscillations and their Relationship, ed. F. P. Pijpers, J. Christensen-Dalsgaard, & C. S. Rosenthal (Kluwer Academic Publishers), 73

Ulmschneider, P. 1994, A&A, 288, 1021

Ulmschneider, P., & Kalkofen, W. 1978, A&A, 69, 407

Ulmschneider, P., Kalkofen, W., Nowak, T., & Bohn U. 1977, A&A, 54 61

Ulmschneider, P., Muchmore, D., & Kalkofen, W. 1987, A&A, 177, 292

Ulmschneider, P., & Musielak, Z. E. 1998, A&A, 338, 311

Ulmschneider, P., Musielak, Z. E., & Fawzy, D. E. 2001, A&A, 374, 662

Ulmschneider P., Theurer J., & Musielak, Z. E. 1996, A&A, 315, 212

Ulmschneider P., Theurer, J., Musielak, Z. E., & Kurucz, R. 1999, A&A, 347, 243

Ulmschneider P., Zähringer, K., & Musielak, Z. E. 1991, A&A, 241, 625

Vernazza, J. E., Avrett E. H., & Loeser, R. 1981, ApJS, 45, 635

Wilson, O. C. 1968, ApJ, 153, 221

Weiss, N. O. 1994, Lectures on Solar and Planetary Dynamos, Ed. M. R. E., Proctor, & A.D. Gilbert (Cambridge Univ. Press), 59

Zhugzhda, Y., Bromm, V., & Ulmschneider, P. 1995, A&A, 300, 302

Ziegler U., & Ulmschneider, P. 1997, A&A, 327, 854